PETER POULAY SPECIAL ISSUE, editor in charge H. F. SCAEFER

The Mechanism of a Barrierless Reaction: Hidden Transition State and Hidden Intermediates in the Reaction of Methylene with Ethene

Hyun Joo,[a] Elfi Kraka,[a⋆], Wolfgang Quapp,[b] and Dieter Cremer[c⋆]

[a] Department of Chemistry, The University of the Pacific, Stockton, CA 95366, USA

ekraka.at.pacific.edu

[b] Mathematical Institute, University of Leipzig, Augustus-Platz, D-04109 Leipzig, Germany

quapp.at.rz.uni-leipzig.de

[c] Department of Chemistry and Department of Physics,

The University of the Pacific, Stockton, CA 95366, USA

dcremer.at.pacific.edu

Abstract: The chelotropic addition reaction of singlet methylene to ethene yielding cyclopropane (reaction 1) was investigated with the help of the Unified Reaction Valley approach (URVA) using different levels of theory (B3LYP, MP2, MP4, CCSD(T), G3) and two basis sets (6-31G(d,p), 6-311++G(3df3pd)). At all levels of theory, reaction (1) proceeds without barrier and transition state (TS). Nevertheless, reaction (1) possesses a distinct mechanism comprising four different reaction phases: 1) a van der Waals phase, in which the stereochemistry of the reaction is decided; 2) an electrophilic attack phase, in which charge is transferred from ethene to methylene to establish a weak bonding interaction between the reaction partners typical of those encountered in TSs of CC bond forming reactions; c) a nucleophilic attack phase, in which charge transfer between methylene and ethene is reverted and a trimethylene biradical structure is formed; d) a ring closure phase, in which the trimethylene structure closes to the three-membered ring. The URVA analysis identifies a hidden TS and two hidden intermediates at the transitions from one phase to the next. If methylene is replaced by difluorocarbene (reaction 2) or germylene (reaction 3), the 4-phase mechanism is retained, however the hidden TS and one of the hidden intermediates are converted into real TS and real intermediate thus establishing 2-step mechanisms with strongly different energy profiles along the reaction path.

Key words: reaction valley approach, barrierless reactions, methylene-ethene system, hidden transition state, hidden intermediates difluoromethylene-ethene system, germylene-ethene system,

1. Introduction

In quantum chemistry, the analysis of the mechanism of a chemical reaction is mostly based on the location and investigation of stationary points along the reaction path on the potential energy surface (PES) of the reaction system. The number of first order saddle points corresponds to the number of transition states (TSs), which in turn indicates whether the reaction follows a one-step (one TS: concerted) or n-step (n TSs with n = 2, 3 ...; non-concerted) mechanism. Calculation of energy, geometry, charge distribution, vibrational frequencies, etc. of the reaction complex (supermolecule formed by the reacting molecules) at the stationary points provides insight into the details of the reaction mechanism. Often there is the need to use the intrinsic reaction coordinate (IRC) approach to determine the topology of the PES and to confirm that the reaction path of a given chemical reaction correctly connects the stationary points under consideration. In the case of more complex reactions, it is a basic requirement of any mechanistic analysis to clarify the connectivity of all TSs located on the PES by appropriate IRC calculations. If the latter are routinely carried out, it will be just a small additional computational investment to perform the Unified Reaction Valley approach (URVA). [1-6] URVA is based on the reaction path hamiltonian (RPH) of Miller, Handy, and Adams, [7] the IRC of Fukui [8,9] and the generalized adiabatic mode concept of Cremer and co-workers. [10,11] URVA leads to a detailed analysis of the reaction mechanism providing information on both electronic and dynamic changes of the reaction complex along the reaction path. For this purpose, the reaction path embedded in the reaction valley is explored in two steps: a) from the location of the TS back into the entrance channel of the reaction and down to the valley minimum occupied by the reacting molecules; b) forward into the exit channel and down to the valley minimum being the location of the product molecules. In case of a multi-step reaction, in which beside reactant- and product minimum also local PES minimum occupied by intermediates are encountered, this procedure is repeated for each TS where the investigated part of the reaction path is limited by the position of minimums directly connected to the TS in question.

In previous work, we found that bond breaking and bond forming are indicated by strong curvature of the reaction path whereas small curvature enhancements are related to the preparation of the reaction complex for the chemical processes. [2,4-6] The height of the curvature peaks can be related to the strength of the bonds being broken/formed, which has an influence on the reaction barrier and the reaction energy. [1,2] Based on the sequence and the position of curvature peaks, a TS region, in which the chemical processes occur, can be distinguished from a) van der Waals regions in entrance and exit channel, in which the first interactions between the reactants forming the reaction complex develop (note that the term reaction complex does not imply the existence of a stable van der Waals complex [1,2]), and b) preparation regions, in which the reactants prepare for the actual chemical processes. [1,2,4-6] We note that a van der Waals region can be observed along the reaction path even if a van der Waals complex does not exist.

The curvature of the reaction path is related to the curvature couplings, which result from a coupling between the vibrational modes orthogonal to the reaction path and the translational mode of the reaction complex along the reaction path. The curvature couplings provide information how energy can be transferred from vibrational modes into the reaction path mode and vice versa, [12,13] which can be used for mode selective rate enhancement. Similarly, analysis of coupling between vibrational modes along the reaction path leads to an understanding of energy dissipation during the reaction.

URVA as any other related mechanistic analysis is based on the existence of a unique reaction path, which is defined by the IRC path being identical to the minimum energy path (MEP). Although just a minority of reacting molecules may follow exactly the MEP for a given temperature larger than zero, knowledge of the MEP is in so far essential as it is representative for all similar paths and therefore the mechanistic analysis has to be carried out just once. This changes in the case of barrierless reactions, which do no longer possess a TS. The MEP (IRC path) depends on the existence of a TS and accordingly a MEP can no longer be determined in the case of barrierless reactions. Accordingly, URVA can only be carried out provided a reasonable alternative to the MEP is found in the case of barrierless reactions so that it is still justified to perform the mechanistic analysis just once and to consider the results of this analysis to be representative for the reaction mechanism.

The problem encountered for the mechanistic analysis of barrierless reactions has to be seen on the background of the fact that many chemical reactions proceed without an activation enthalpy although reliable quantum chemical methods suggest the existence of a small barrier and by this a TS. Such a TS can be used for the calculation of MEP and the mechanistic analysis despite lack of any chemical relevance of barrier and TS. The MEP obtained for these reactions are still representative for many other similar reaction paths followed by the reaction complex in a statistical manner.

If a TS does not exist at all, it will be necessary to obtain an insight into some basic features of the PES concerning the barrierless reaction in question. It has to be clarified whether there is still a reaction valley that starts at the minimum of the reactants and terminates at an energy plateau as it is the case for many dissociation reactions. In recent work, [14] we have demonstrated that the PES can be systematically explored with the help of Newton trajectories (NTs; originally coined reduced gradient following curves). [15,16] NTs have the property of connecting the valley minimum with the energy plateau of a barrierless reaction where the NTs, despite of different starting directions, bundle in the exit channel of the valley before it merges into the energy plateau. [14] It has been shown that the bundling of NTs can be used to determine a starting point for a path downhill from the energy plateau to the minimum. The path follows the valley floor and by this provides a reasonable and representative reaction path, along which the mechanistic analysis can be performed. [14]

There are however also situations where the reaction valley is no longer distinctive but opens to a broad bowl leading up to the energy plateau as found in the case of a cirque created by a mountain glacier. [14]

Again, the basic features of such a cirque can be explored with the help of NTs and again it is possible to define a reasonable reaction path, along which a representative mechanistic analysis can be carried out.

In previous work, we have discussed the computational implications of determining for a barrierless reactions a reasonable reaction path. In the current work, results of the previous study are utilized to answer the basic question whether analysis of the mechanism of a barrierless reaction can be of any general use. As a suitable barrierless reaction we investigate the chelotropic addition of singlet methylene, $CH_2(^1A_1)$, to ethene thus yielding cyclopropane (reaction 1, Scheme 1a). The chelotropic reactions between carbenes and alkenes have been investigated numerous times in the last 50 years [17-30] ever since Skell [17,19] and later Doering [18] provided the first experimental evidence for a two-step mechanism of these reactions. In the first step (see Scheme 1c), the vacant pπ-orbital of the carbene interacts with the π-bond of the alkene in an electrophilic manner, which implies a non-linear approach of the carbene to the alkene. In the second step, the electrophilic attack is followed by a nucleophilic attack involving the occupied (sp^2-hybridized) lone-pair orbital of singlet carbene after reorientation of the carbene in a more perpendicular manner relative to the double bond (Scheme 1c). Hence, the carbene-alkene reactions follow a non-least motion (non-linear) rather than a least motion (linear) path, which is in line with the theory of symmetry-allowed and symmetry-forbidden chelotropic reactions. [31] Early theoretical support for this mechanism was provided by Hoffmann [21] who used semiempirical Extended Hückel calculations for an investigation of reaction (1). Experimental proof for the non-least motion path turned out to be more difficult, however Houk and co-workers [32] succeeded in providing such proof on the basis of kinetic isotope measurements and quantum chemical calculations in the case of the addition of CCl_2 to pent-1-ene.

After sophisticated quantum chemical calculations of the ab initio or density functional (DFT) type became generally available, reactions between ethene and $CH_2(^1A_1)$ [23-25,30] or other carbenes CX_2 ($X \neq H$) [26-30] were investigated and described in more detail. These investigations focused exclusively on the energetics of the carbene addition reactions, their stereochemistry, and the description of the stationary points along the reaction path. So far, a complete mechanistic analysis as it can be obtained by utilizing URVA or similar methods based on the RPH is not available. In the case of reaction (1), a two-step mechanism is not possible because of the missing barrier. Nevertheless, one assumes (without actual proof) a similar reaction mechanism as for other carbene addition reactions. Apart from this, it is a general tendency among chemists to consider barrierless reactions as less interesting.

We will show in this work that a barrierless reaction such as (1) can possess a complicated reaction mechanism, which provides detailed information about other chelotropic addition reactions of the same type. Furthermore, we will demonstrate that a TS encountered for other carbene-alkene addition reactions becomes already obvious from the analysis of the barrierless reaction (1). We will develop in this connection the concept of a "hidden TS" that properly complements the concept of "hidden intermediates" previously established in connection with the mechanistic analysis of symmetry-forbidden reactions. [4] For the purpose of testing predictions made on the basis of the mechanistic analysis of reaction (1), we will investigate two other chelotropic reactions, namely the addition of singlet difluoromethylene to ethene (reaction 2) [22,26-29] and of singlet germylene to ethene (reaction 3, see Scheme 1), [30] which represent to characteristic opposing cases that can be anticipated once the mechanism of (1) is understood.

Scheme 1

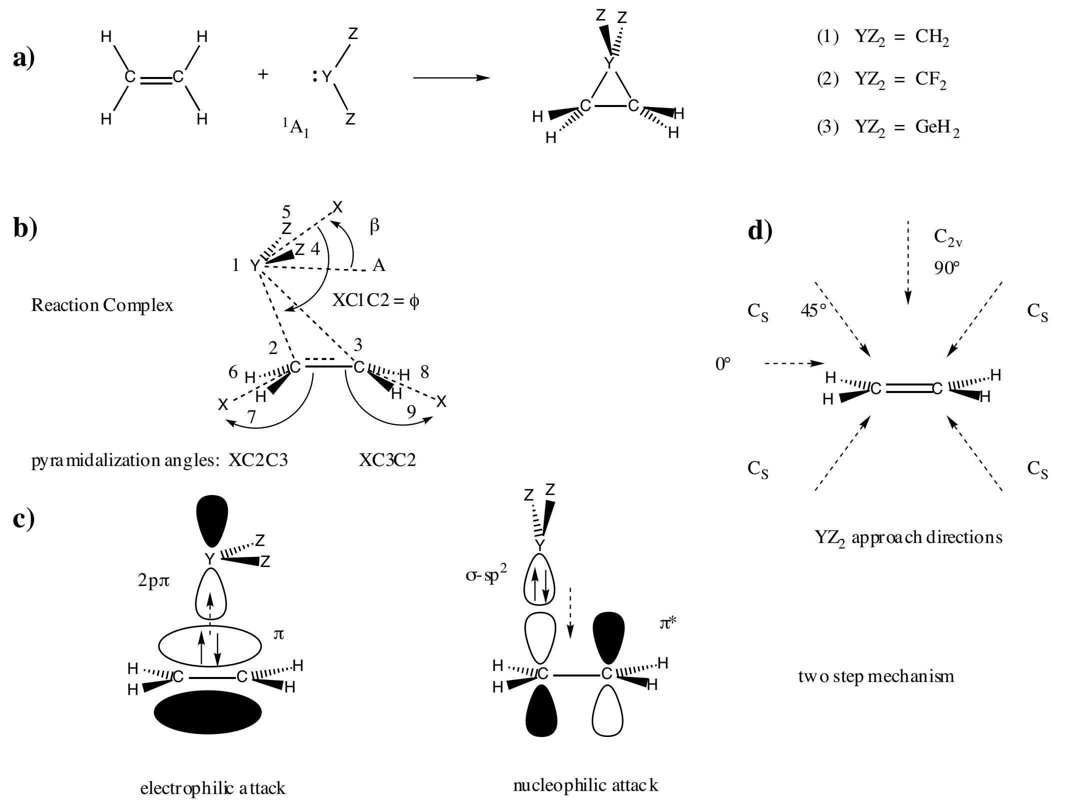

Scheme 1. a) Reactions (1), (2), and (3) investigated. b) Reaction complex: numbering of atoms and definition of internal coordinates used for its description. c) Two step mechanism with electrophilic and nucleophilic attack. d) Possible approach directions of YZ_2 (relative to ethene) and resulting symmetries of the reaction complex.

Results of this work will be discussed in four sections. In Section 2, we will shortly describe the theory of URVA and the computational methods used in this work. In Sections 3, 4, and 5, the URVA analysis of reactions (1), (2), and (3) will be presented and discussed. The chemical relevance of results is discussed in Section 6 where also conclusive remarks and an outlook on future work in connection with the concepts of hidden TSs and hidden intermediates are given.

2. Theory and Computational Methods

URVA [1,2] is based on a partitioning of the 3K-L-dimensional configuration space (L: number of overall rotations and translations, K: number of atoms) of the reaction complex into a one-dimensional reaction path space, along which the translational motion of the reaction complex takes place, and a (3K-L)-1-dimensional orthogonal space, in which the vibrations of the reaction complex orthogonal to the reaction path movement occur. In this way, one distinguishes between the path along the valley floor and the shape of the valley in the transverse directions when following the reaction path from reactants to products.

The quantities used for describing reaction path and reaction valley have been described in previous work [1,2,4-6] and therefore, we will outline here just some essential features of URVA. The IRC path is the steepest descent path expressed in mass-weighted coordinates. [8,9] It is defined by the line $\tilde{\mathbf{x}}(s)$, which is given as a column vector of 3K mass-weighted Cartesian coordinates $\mathbf{x_i}$. The tilde is used to indicate mass-weighting. The reaction path is given parametrically in terms of its arc length s defined by the differential

$$ds^2 = d\mathbf{x}^\dagger \mathbf{M} d\mathbf{x} = d\tilde{\mathbf{x}}^\dagger d\tilde{\mathbf{x}} \tag{1}$$

with $\mathbf{M}$ being the diagonal matrix of nuclear masses. The direction of the reaction path $\tilde{\mathbf{x}}(s)$ is determined by the reaction path vector $\mathbf{t}(s)$ identical to the normalized energy gradient vector $\tilde{\mathbf{g}}(\tilde{\mathbf{x}}(s))$.

Eq. (2) describes the *harmonic* reaction valley.

$$V(s, \mathbf{Q}) = V(s) + 1/2 \sum_{\mu=1}^{N_{vib}} k_\mu^g(s) \quad \bullet \quad [Q_\mu^g(s)]^2 \tag{2}$$

where $k_\mu^g(s)$ and $Q_\mu^g(s)$ are generalized normal mode force constant and generalized normal mode coordinate, respectively, for generalized normal mode $\tilde{\mathbf{l}}_\mu^g(s)$ with frequency $\omega_\mu^g(s)$ (N_{vib} = (3K-L)-1); $V(s)$ gives the energy profile along the reaction path. The exchange of energy between reaction path mode and transverse vibrational modes can be studied provided curvature vector $\mathbf{k}(s)$, scalar curvature $\kappa(s)$, and curvature coupling elements $B_{\mu,s}(s)$ are known. Mode-mode coupling elements $B_{\mu,\nu}(s)$ provide an insight into energy dissipation. [1,12,13] The curvature coupling elements $B_{\mu,s}(s)$ represent coefficients of the expansion of the curvature vector in terms of generalized normal modes.

By graphically presenting the scalar curvature $\kappa(s)$ one can locate its maxima along the reaction path, which indicate those points where energy can flow from one (or more) of the transverse normal vibrational modes into the motion along the reaction path (or vice versa). Increased curvature of the path is always indicative of changes in the geometry of the reaction complex and reflects major electronic changes. Apart from this, it has dynamic consequences: The reaction rate can be enhanced by pumping energy (with the help of a laser) in that particular vibrational mode, which couples with the motion along the reaction path (*mode selective rate enhancement* [12]). In previous work we have shown that mode selective rate enhancement can be successfully applied to symmetry-forbidden reactions, [4] however is of little or no use in the case of symmetry-allowed reactions, [5] which follow a reaction path without large curvature peaks in entrance channel or TS region. This is also true for the reactions studied in this work and therefore we will analyze the reaction path curvature in terms of generalized adiabatic vibrational modes rather than generalized normal vibrational modes (needed for mode selective rate enhancement) because the former are more suitable for a mechanistic analysis.

Any normal vibrational mode can be expressed in terms of adiabatic vibrational modes. [10,11] An adiabatic internal vibrational mode is described by the mode vector $\mathbf{a}_n$ and corresponds to an elementary vibrational mode associated with an internal coordinate q_n as for example bond length, bond angle or dihedral angle. [10,11] Adiabatic modes are based on a dynamic principle (leading parameter principle [5]) and are directly obtained from a modified form of the Euler-Lagrange equations. [10] They are perfectly suited to characterize normal vibrational modes in the common language of chemistry that attempts to express molecular properties in terms of internal coordinates q_n.

The reaction path curvature can be analyzed utilizing the amplitude $A_{n,s}(s)$ [1,2]

$$A_{n,s}(s) = \frac{\mathbf{k}(s)^\dagger \mathbf{M}(s) \mathbf{a}_n^g(s)}{\sqrt{(\mathbf{a}_n^g)^\dagger \mathbf{M}(s) \mathbf{a}_n^g(s)}} \tag{3}$$

which characterizes the curvature vector $\mathbf{k}(s)$ in terms of generalized adiabatic modes associated with the internal coordinates describing the reaction complex. The curvature coupling coefficients $A_{n,s}$ possess the same dimension as coefficients $B_{\mu,s}$.

In a similar way as the curvature vector $\mathbf{k}(s)$, also the reaction path vector $\mathbf{t}(s)$ can be decomposed into a set of basis vectors $\mathbf{u}_n(s)$ associated with the internal coordinates of the reaction complex. Vectors $\mathbf{u}_n$ are internal modes that characterize the movement of the reaction complex along the reaction path and, therefore, they play a similar role for the translational movement as the adiabatic internal modes do in the analysis of the transverse normal mode vibrations. [1,2] The reaction path vector is analyzed with the help of amplitudes $A_{n,s}(\mathbf{t}, s)$

$$A_{n,s}(\mathbf{t}, s) = \frac{(\mathbf{g}^\dagger \mathbf{M}^{-1} \mathbf{b}_n)^2}{(\mathbf{g}^\dagger \mathbf{M}^{-1} \mathbf{g})\ \ (\mathbf{b}_\mathbf{n}^\dagger \mathbf{M}^{-1} \mathbf{b}_n)} \tag{4}$$

($\mathbf{g}$: gradient; an element i of the vector $\mathbf{b}_n$ is given by $\partial q_n(\mathbf{x})/\partial x_i$) which considers (beside electronic effects) the kinetic aspect of the translational motion along the reaction path. [1,2]

Four different levels of theory ranging from Møller-Plesset (MP) perturbation theory [33] at second (MP2) and fourth order (MP4) to DFT [34] and Coupled Cluster (CC) theory [35] with all single (S) and double (D) excitations and a perturbative inclusion of the triple (T) excitations (CCSD(T) [36]) were applied to investigate the stationary points along the path of reactions (1), (2), and (3). These methods were complemented by the use of G3. [37] Two basis sets were used for this purpose, namely Pople's 6-31G(d,p) basis set (henceforth called basis A) [38] and the augmented VTZ+P basis 6-311++G(3df,3pd) (basis B). [39] In the case of the DFT calculations, Becke's hybrid functional B3LYP [40] was applied despite its shortcomings in the case of van der Waals complexes and the underestimation of TS energies. [41] Previous investigations have revealed that quantum chemical errors in the prediction of the energetics of chemical reaction do not spoil the mechanistic analysis of a reaction, which can be reproduced even with a minimal basis set at the Hartree-Fock level. [2,4,5]

Vibrational frequencies were calculated at the MP2 and B3LYP levels of theory with both basis A and B, respectively, to verify the nature of the stationary points in reactions (1), (2), and (3) and to calculate thermochemical data such as activation enthalpies $\Delta H^a(298)$ and reaction enthalpies $\Delta H(298)$. - The basis set superposition error (BSSE) [42] was corrected with the help of the counterpoise method [43] to assess the stability of a van der Waals complex more accurately. - The charge transfer from or to ethene was calculated using the natural bond orbital (NBO) analysis. [44]

The internal coordinates describing the reaction complex are given in Scheme 1b. The same internal coordinates were used to define the adiabatic vibrational modes with the exception of the pyramidalization angles ϕ(XY1C2) = XY1C2, ϕ(XC2C3) = XC2C3, and ϕ(XC3C2) = XC3C2, which were replaced in the URVA calculations by the dihedral angles Z4Y1Z5C2 = ZYZC, H6C2H7C3 = HC2HC, and H8C3H9C2 = HC3HC, respectively. In addition, we used the angle β defined in Scheme 1b as a geometrical indicator of the electrophilicity of YZ_2 as was originally suggested by Houk and co-workers. [26]

Exploratory investigations of the reaction path were carried out at the B3LYP/A level of theory using a constant step length of 0.05 amu$^{1/2}$ Bohr. Then, calculations were repeated at the same level of theory reducing the step size to 0.03 amu$^{1/2}$ Bohr or smaller values in connection with the diabatic mode ordering (DMO) procedure of Konkoli, Cremer, and Kraka. [2] DMO resolves all avoided crossings of the vibrational modes along the reaction path and in this way a reliable analysis of curvature coupling and mode-mode coupling coefficients becomes possible. For each value of the reaction coordinate s, the reaction path vector $\mathbf{t}$(s) and its decomposition in terms of internal coordinate modes $\mathbf{u}_n$, the forces exerted on the atoms of the reaction complex, the 3K-7 generalized normal modes $\mathbf{l}^g_\mu(s)$ with associated frequencies ω^g_μ(s), the decomposition of $\mathbf{l}^g_\mu(s)$ in terms of generalized adiabatic internal modes $\mathbf{a}^g_n(s)$, the adiabatic force constants k^a_n associated with the internal coordinates given in Scheme 1, reaction path curvature κ(s), coupling coefficients B_μ, s and $B_{\mu,\nu}$, NBO charges, and the electron density distribution $\rho(\mathbf{r}, s)$ were calculated.

The topology of the PESs associated with reaction complexes (1), (2), and (3) was explored with the help of NTs. [15,16] Details of these calculations can be found elsewhere. [14] It turns out that the PES of reaction complex (1) has the shape of a cirque (Figures 1a and 1b), i.e. there is no longer a distinctive reaction valley leading to the energy plateau occupied by the reaction partners methylene and ethene, but a broad slope connecting the valley minimum to the energy plateau as found for a bowl with a horizontally curved bowl edge. Based on the possible symmetries of the reaction complex one can distinguish three different situations: a) The reaction complex possesses C_{2v} symmetry throughout the reaction leading to cyclopropane, i.e. methylene approaches ethene along the bisector passing through the midpoint of the a)

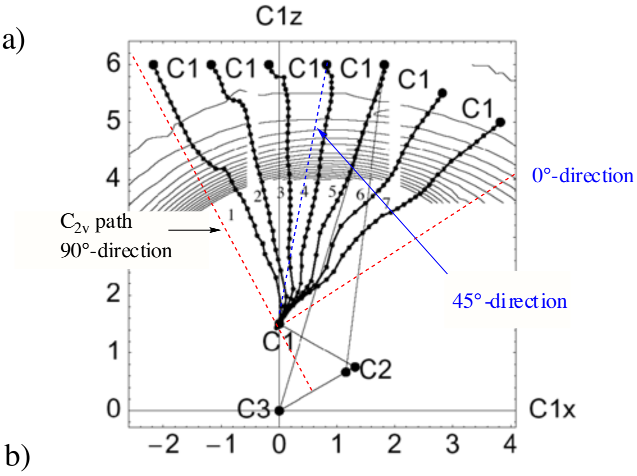

b)

Figure 1. **a)** Calculated NTs for the C_s-symmetrical cycloaddition of singlet methylene to ethene as described with B3LYP/A shown in a 2D subspace spanned by the x- and the z-coordinate of the methylene atom C1 where the origin of the coordinate system is given by ethene atom C3. The starting geometry of one reaction complex is sketched as well as the cyclopropane geometry at the end point of one NT (marked by larger dots). Smaller dots along the NT correspond to intermediate C1 positions, which imply small shifts in the position of C2 for a fixed position of C3. Each dot is one node point of the NT. Also shown are parts of the PES in form of contour line diagrams in a region where the valley smoothly disembogues into the plateau (109 to 112 kcal/mol above cyclopropane). Changes in the energy on the energy plateau are so small that contour lines and NT paths become erratic. All calculated NTs (up to 33 node of the GS calculated) are on the right side of the C_{2v}-symmetrical symmetry-forbidden path (90°-direction) where the two NTs closest to this path (NT1 and NT2) are effected in the way that they do no longer decrease monotonically but have to surmount first small hills in the region of the plateau. All other NTs possess monotonically decreasing energy profiles. Over a range of 50 degrees they behave in the same way and indicate thereby the existence of a cirque rather than a valley. As starting point for the URVA calculations point C1 of NT 4 (45°-direction) was taken. - **b)** Photography of a cirque with a similar topology than the PES of reaction (1) (courtesy of Dr. W. W. Locke, Montana State University).

double bond (90°-direction; Figure 1a, Scheme 1d). b) The methylene group can approach ethene along a path parallel to the ethene double bond (0°-direction, Figure 1a, Scheme 1b) where the reaction complex adopts C_s-symmetry. Depending on the distance from the ethene double bond, trimethylene can be formed, which then closes to cyclopropane. c) Between extremes a) and b) there is an infinite number of reaction paths with directions between 0 and 90° for a C_s-symmetrical methylene approach. In view of the fact that the PES has the shape of a cirque in this area (Figure 1a), a reasonable reaction path for the mechanistic analysis was defined by the 45° approach direction, i.e. the starting point of the URVA calculations was taken in the 45° direction at a distance 4.2 Å apart from C2. Note that the NT started at the same point does not necessarily follow the steepest descent path to cyclopropane (see Figure 1a). - For reactions (2) and (3), a TS was found in each case, so that a unique reaction path could be defined via the MEP.

All calculations needed for URVA were carried out with the program ADIA, which is a multiporpose package for the analysis of vibrational spectra and carrying out URVA calculations. [2,10,11] ADIA is a part of the ab initio package COLOGNE2007. [45] For the DFT and CCSD(T) calculations, the ab initio packages GAUSSIAN03 [46] and a local version of ACESII [47] were used.

3. Mechanism of the Chelotropic Addition of Methylene to Ethene

The addition of $CH_2(^1A_1)$ to $H_2C{=}CH_2$ leading to cyclopropane is symmetry-allowed when proceeding in a non-linear C_s-symmetrical fashion where in this work the 45°-approach direction was chosen (see above). At all levels of theory considered, the reaction proceeds without a barrier and is strongly exothermic. Calculated reaction energies ΔE vary from -119.5 (MP2/B), -112.1 (B3LYP/A), -105.6 (B3LYP/B), -107.1 (CCSD(T)/B) to -108.9 kcal/mol (G3, Table 1), which correspond to reaction enthalpies ΔH(298) at 298 K of -113.5 (MP2/B), -105.5 (B3LYP/A), -99.3 (B3LYP/B), -100.8 (CCSD(T)/B) and -100.8 kcal/mol (G3). The experimental reaction enthalpy ΔH(298) is 101.5$\pm$0.7 kcal/mol as derived from standard heats of formation for ethene and cyclopropane, [48] and the heat of formation of 101.8 $\pm$0.5 for $CH_2(^1A_1)$. [49] CCSD(T) and G3 lead to a reliable description of reaction (1). The MP2 value differs by 12 kcal/mol whereas the B3LYP differ by 2 - 4 kcal/mol indicating a reasonable agreement between theory and experiment.

We explored the symmetry-forbidden C_{2v}-symmetrical (90°-direction) approach path with CASSCF and CASPT2 calculations and found a second order TS (two imaginary frequencies corresponding to a translational movement along and perpendicular to the C_{2v} path) about 16 kcal/mol above the energy of the separated reactants. A second order TS has no relevance for the reaction mechanism and therefore, the PES was not further investigated in this direction.

For the 45°-path, the parameter $s = 0$ amu$^{1/2}$ Bohr was chosen for a C1C2 distance of 4.224 Å clearly outside the van der Waals distance between two C atoms (2 $\times$ 1.8 = 3.6 Å [50]) and corresponding to an energy just 0.1 kcal/mol below the sum of the energies of the reaction partners at infinite separation. This energy difference happens to be equal to the BSSE calculated for the separated reactants in the geometry of the reaction complex at $s = 0$ amu$^{1/2}$ Bohr. At this distance, the geometries of the monomers are largely intact (changes in bond lengths and angles smaller than 0.01 Å and 0.5°, respectively). The endpoint of the reaction path was located at $s = 19.56$ amu$^{1/2}$ Bohr, which is the location of cyclopropane.

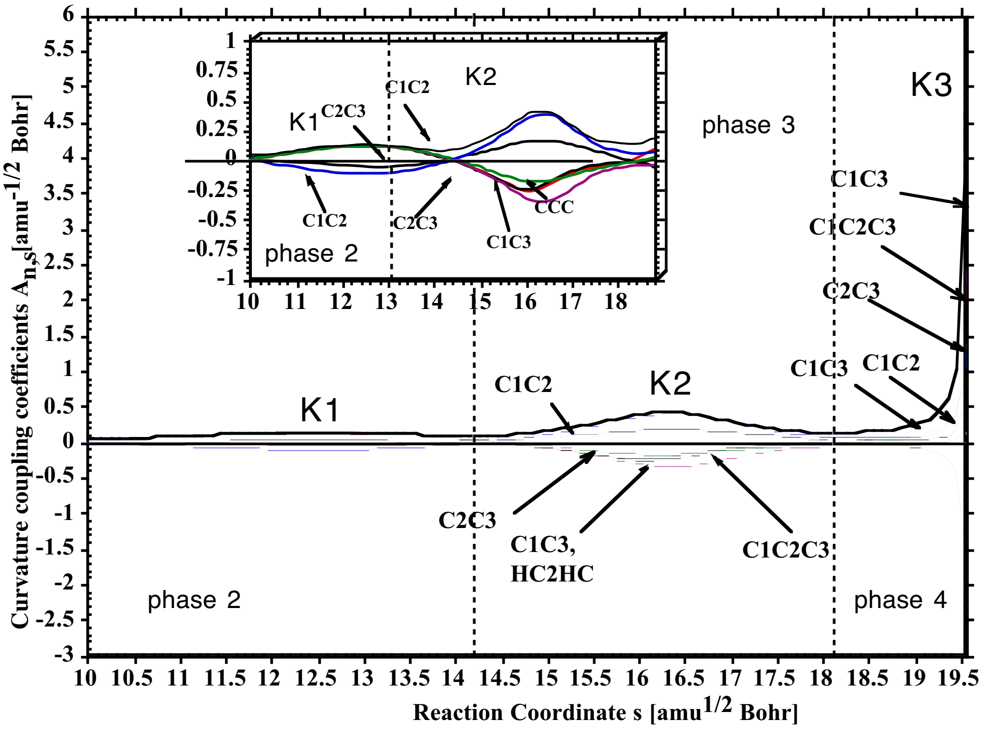

Figure 2. Decomposition of the scalar reaction path curvature κ(s) (thick solid line) in terms of adiabatic mode-curvature coupling amplitudes $A_{n,s}$(s) (thin lines). A redundant coordinate set was used for the analysis (Scheme 1b). Curvature enhancements K1, K2 and peak K3 and reaction phases 2, 3, and 4 are indicated. The insert gives an enlargement of the curvature diagram in the range $s = 10$ to $s = 18.8$ amu$^{1/2}$ Bohr. In both diagrams, reaction phases are indicated. B3LYP/6-31G(d,p) calculations.

In Figure 2, the scalar reaction path curvature $\kappa(s)$ of reaction (1) is shown for the range $s = 10$ to 19.5 amu$^{1/2}$ Bohr. Curvature enhancements K1 and K2 or peak K3 indicate weaker or stronger changes in the reaction complex and coupling of the translational motion along the reaction path with the vibrational modes in the space orthogonal to the reaction path. K1 and K2 are typical of electron reorganization proceeding the actual bond forming (breaking) steps as found for symmetry-allowed chemical reactions such as the Diels-Alder reaction. [5] The distinctive curvature peak K3 indicates the bond forming process leading to the three-membered ring.

In previous work, [1,2,4-6] we have demonstrated that the curvature peaks (enhancements) along a reaction are the basis for a partitioning of the reaction mechanism into different phases each of which is typical of a distinctive electronic, geometrical, and or dynamic change in the reaction complex. This is also the basis for a dissection of the mechanism of reaction (1) into four phases. (We prefer to use the term reaction phase rather than reaction step to avoid confusions with regard to the concerted or non-concerted character of a reaction. A reaction phase is defined by the minimums in the reaction path curvature and other path-typical properties.) In the following, we will discuss the mechanism phase by phase, utilizing besides the curvature diagram (Figure 2) also Figures 3a, 4a, and 5a, which give snapshots of the geometry at characteristic points along the path (Figure 3a), the charge transfer between the reaction partners (Figure 4a) and the changes in the pyramidalization angles as a function of the path parameter s (Figure 5a).

Phase 1: van der Waals range. As shown in Figure 3a for $s = 0$ amu$^{1/2}$ Bohr, methylene approaches ethene sidewards with its H atoms first (tail-on rather than head-on). In previous work, this approach mode has been considered as a necessity of an electrophilic attack of methylene. [21] We note however that for $s = 0$ amu$^{1/2}$ Bohr, there is only little charge transfer (Figure 3a, Figure 4) between the molecules (1 melectron). More important are the electrostatic interactions between the molecules involving the dipole moment of CH_2 (B3LYP/6-31G(d,p): 1.79 Debye; positive end: H atoms; negative end: C atom) and the group moment of the nearest ethene CH_2 group. This interaction will only be attractive if methylene approaches ethene tail-on rather than head-on as indicated in Figure 3a for $s = 0$ amu$^{1/2}$ Bohr.

In the range $s = 0$ to $s = 4$ amu$^{1/2}$ Bohr, charge transfer from ethene to the empty 2pπ orbital of methylene is below 10 melectron (Figures 3a and 4a), changes in the geometries of the reaction partners are below 0.001 Å and 1°, and the reaction path curvature is essentially zero. We call phase 1 the van der Waals range of reaction (1) because all interactions of the reaction partners are of the van der Waals type leading to a stabilization of just 1.7 kcal/mol maximally. Although the van der Waals interactions are not relevant for the chemical processes such as bond forming (breaking), they are important with regard to the stereochemistry of the reaction. In the case of (1), they orient the reaction partners in such a way that charge transfer form ethene to methylene becomes possible.

Phase 2: Electrophilic attack range. Phase 2 stretches from $s = 4$ amu$^{1/2}$ Bohr, where the first curvature enhancement starts to develop, to K1 at $s = 12.6$ amu$^{1/2}$ Bohr and to the curvature minimum at $s = 14.4$ amu$^{1/2}$ Bohr (Figure 2) over a total range of 10 amu$^{1/2}$ Bohr. At the end of phase 2, the reaction complex has covered 74 % of the total path, however the energy has been lowered by just 35 % (-40 kcal/mol, Figure 3a) and the C2C3 bond length increased by just 47 % to 1.409 Å (Figure 3a). All this is indicative of a very slow change in stability and geometry of the reaction complex as also documented by the pyramidalization angles (Figure 4a). The angle β (and with it the pyramidalization angle XC1C2 that is parallel to β because of the nearly constant value of angle AC1C2, see Scheme 1b) reveals that methylene remains throughout phase 2 almost in the same orientation relative to ethene. In this period, charge transfer from ethene to methylene increases to a maximum of 100 melectron at $s = 12.6$ amu$^{1/2}$ Bohr (Figure 4a), which happens

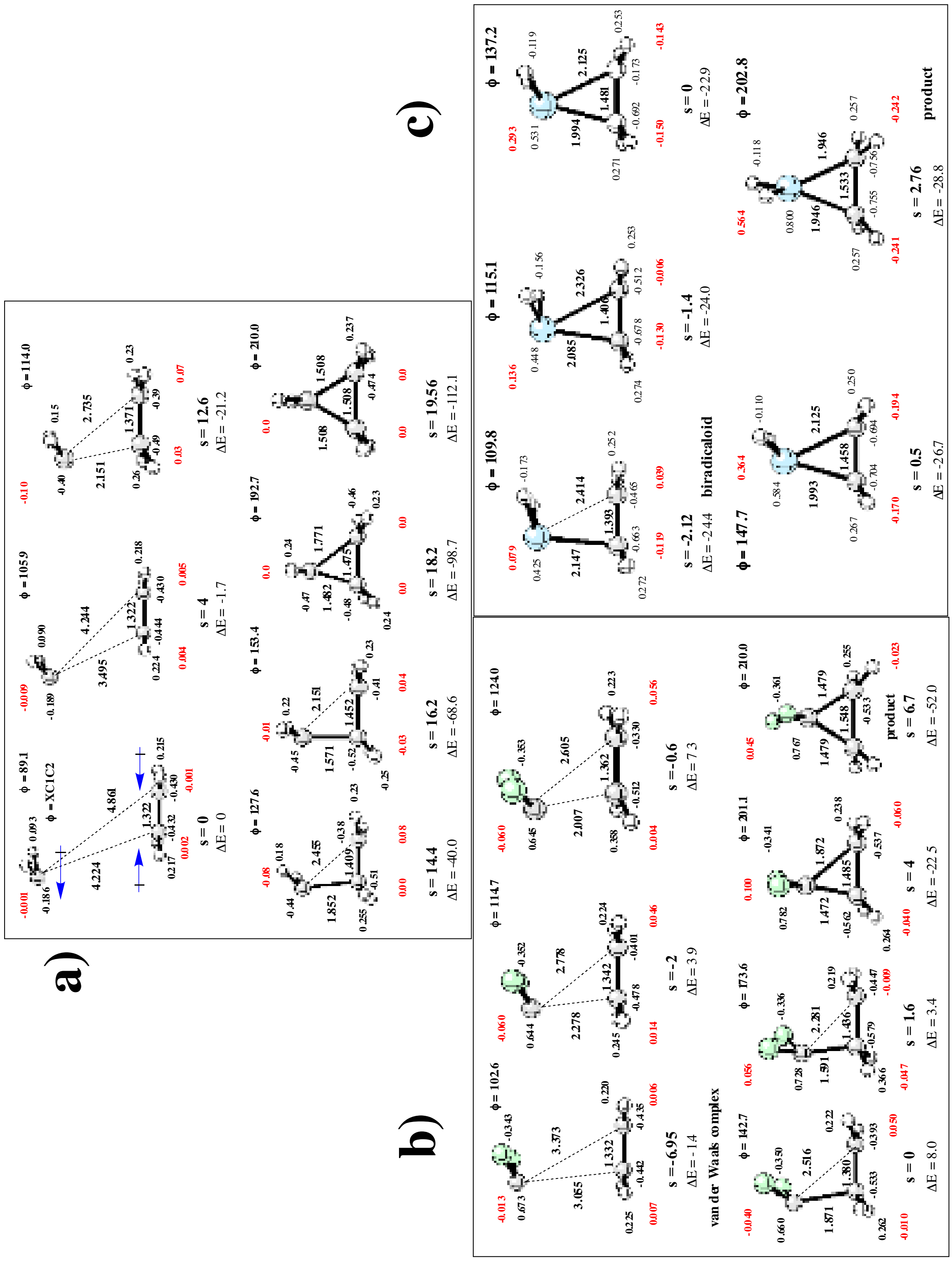

Figure 3. Geometry and NBO charges of the reaction complex at distinctive points s along the reaction path defined by the minima and maxima of the curvature diagram of **a)** reaction (1), **b)** reaction (2), and **c)** reaction (3). For $s = 0$ amu$^{1/2}$ Bohr (Figure a), the dipole moment of methylene and the group moments (both in blue) of the ethene CH_2 groups are indicated (chemical notation). The NBO charges are given for each atom in small black print and the resulting group charges determining the charge transfer in red print. Bond lengths in Å, angles in degree, NBO charges in electron. B3LYP/6-31G(d,p) calculations.

to be the position of the curvature enhancement K1 (Figure 2), i.e. within phase 2 this is the position of both a maximum charge transfer, the strongest changes in the geometry, and the most significant coupling of translational and vibrational motions of the reaction complex. We note that at this point the charge polarization of the bond C2C3 is also strongest generating in this way a partially positive atom C3 and a partially negative atom C2 (see Figure 3a).

It is interesting to note that within phase 2, methylene remains in a configuration that orients orbital 2pπ(C1) more in the direction of C3 rather than C2 although the distance C1C3 is 0.6 Å larger than the distance C1C2. This configuration is not optimal for a CH_2 unit with frozen orbitals, however suitable for the rehybridization process and the charge reorganization CH_2 has to undergo. At the end of phase 2, the reaction complex adapts a geometry (C1C2: 1.852 Å, Figure 3a) typical of a TS, in which a short C1C2 bond is established.

At s = 14.4 amu$^{1/2}$ Bohr (Figure 2), the electrophilic attack seems to be finished as suggested by the following observations: a) The scalar curvature adapts a minimum value; b) adiabatic curvature couplings for internal coordinates C1C2, C1C3, C2C3, angles C1C2C3 and the two pyramidalization angles HC2HC3 and HC3HC2 change their sign; c) charge transfer between ethene and methylene has been reverted, i.e. there is a back-transfer of negative charge from the CH_2 group to the ethene molecule. In line with these observations and the original mechanism of Skell, Doering, Hoffmann, Houk and others, [17-22,26,27] we call phase 3 of reaction (1) the nucleophilic attack range of the negatively charged carbene on the positively charged ethene atom C3.

Phase 3: Nucleophilic attack range. This stretches from the curvature minimum at s = 14.4 amu$^{1/2}$ Bohr via K2 positioned at s = 16.2 amu$^{1/2}$ Bohr to the next curvature minimum at s = 18.2 amu$^{1/2}$ Bohr. In this range, methylene changes from an electrophile to a weak nucleophile (maximum back transfer of negative charge: 10 melectron; see Figures 3a and 4a) where K2 gives the position of change from electrophile to nucleophile (Figure 4a). The energy of the reaction complex decreases in phase 3 by another 60 kcal/mol, which indicates that along a path length of just 4.2 amu$^{1/2}$ Bohr electronic, geometric, and dynamic changes are substantial. They include rehybridization and reorganization of charge especially in the methylene unit.

The nucleophilic attack implies a reorientation of CH_2 in such a way that angle XC1C2 widens from 128° (s = 14.4 amu$^{1/2}$ Bohr) to 193° (s = 18.2 amu$^{1/2}$ Bohr; for the D_{3h}-symmetrical form of cyclopropane this angle becomes 180 + 30 = 210°). This indicates that backdonation can only proceed effectively after forming the Walsh orbitals of a 3-membered ring, which implies reorientation of CH_2. During the nucleophilic step, the C1C2 distance reduces from 1.852 to 1.482 and distance C1C3 from 2.455 to 1.771 Å. Hence, the C1C2 bond is fully established and at the same time the C2C3 distance lengthens to a comparable value. Parallel to the C1C2 distance reduction, which can also be expressed by a narrowing of the angle C1C2C3, the C2-C3H_2 group pyramidalizes (see Figure 5a). At s = 18.2 amu$^{1/2}$ Bohr, a distorted trimethylene biradical

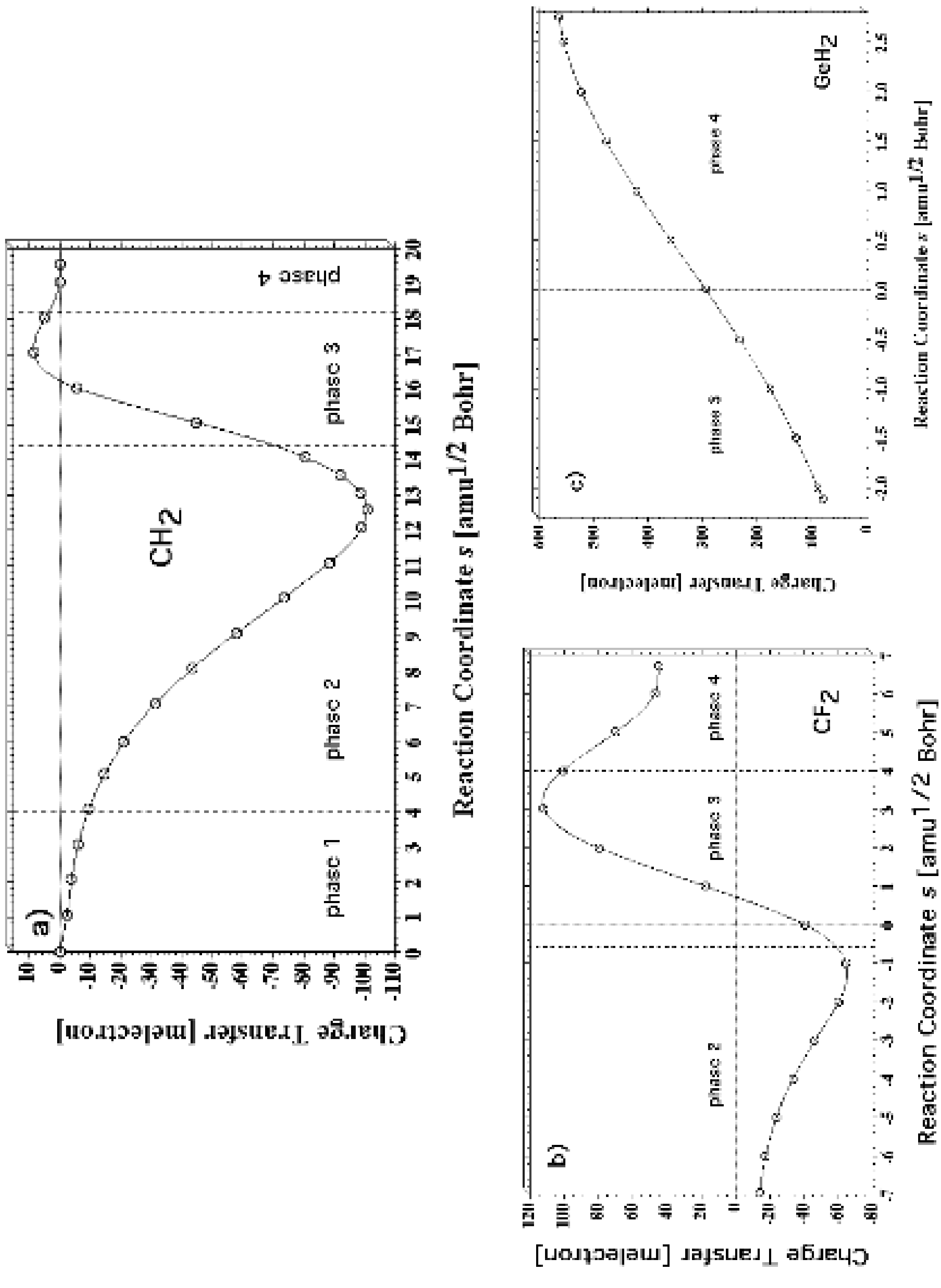

Figure 4. Charge transfer (in melectron) between ethene and YZ_2 according to NBO/B3LYP/6-31G(d,p) calculations as a function of the reaction path parameter s. **a)** CH_2: reaction (1); **b)** CF_2: reaction (2); **c)** GeH_2: reaction (3). - Negative (positive) charge transfer values indicate that YZ_2 accepts (donates) negative charge from (to) ethene. The position of the TS ($s = 0$ amu$^{1/2}$ Bohr) is indicated by a dashed vertical line.

structure with a much too small C1C2C3 angle (74°; C1C3 = 1.771 Å) is formed as a precursor to the final product cyclopropane.

Phase 4: Ring closure range. Phase 4 stretches just by 1.36 amu$^{1/2}$ Bohr from $s = 18.2$ to 19.56 amu$^{1/2}$ Bohr causing in this range an energy lowering of 13 kcal/mol to reach cyclopropane at the endpoint of the path. The bond C1C3 is formed in phase 4 accompanied by an adjustment of the other CC bonds to the cyclopropane values. The decomposition of the scalar curvature in terms of adiabatic curvature coupling coefficients (Figure 2) confirms that peak K3 is associated with stretching modes C1C3, C1C2, and C2C3, which describe the formation of the cyclopropane ring where as an alternative for C1C3 also the bending angle C1C2C3 can be taken (see Figure 2). The adiabatic curvature coupling C1C3 (or C1C2C3) dominates the other curvature couplings. Charge transfer reduces to a zero value and the pyramidalization angles adapt their final values (Figures 4a and 5a.

Total Mechanism. Curvature enhancements K1, K2, and peak K3, denote the chemically relevant phases of the mechanism: electrophilic, nucleophilic, and ring closure phase. The reaction complex enters the electrophilic phase after its stereochemistry has been predetermined in the van der Waals range. In so far, the van der Waals phase cannot be excluded from the mechanistic analysis of reaction (1). One may argue whether it is justified to fix the change from van der Waals to electrophilic attack phase at $s = 4$ amu$^{1/2}$ Bohr. However, even with the use of other criteria setting the start of phase 2 at a higher s value it remains a fact that the electrophilic phase is the longest characterized by a slow and collective change in the geometrical parameters of the reaction complex. This is typical of all symmetry-allowed pericyclic reactions. For example, the mechanism of the Diels-Alder reaction [5] and reaction (1) are similar in the range before the maximal curvature peak K3.

The 4-phase mechanism found for reaction (1) is largely confirmed by other properties of the reaction complex recorded along the reaction path. For example, Figure 6 gives the internal coordinate contributions projected out of the reaction path vector calculated for the range $s = 10$ to $s = 19.56$ amu$^{1/2}$ Bohr. Different parameters dominate the reaction path direction in different phases of the mechanism where distance C1C3 adapts two different roles. In phase 1 (not shown), C1C3 is a simple approach parameter without any chemical relevance. In phase 2 (electrophilic attack), distance C1C2 replaces C1C3 and dominates at the end of phase 2 the reaction path direction (Figure 6). In phase 3, C1C3 becomes a bond parameter and takes over the role of C1C2 with regard of the reaction path direction. The importance of C1C3 is reduced in phase 4 and replaced by the angle C1C2C3, which is most important for the final closing of trimethylene to cyclopropane. Other internal coordinates such as the pyramidalization angles contribute modestly to the reaction path direction (Figure 6).

Based on this 4-phase mechanism three questions emerge:

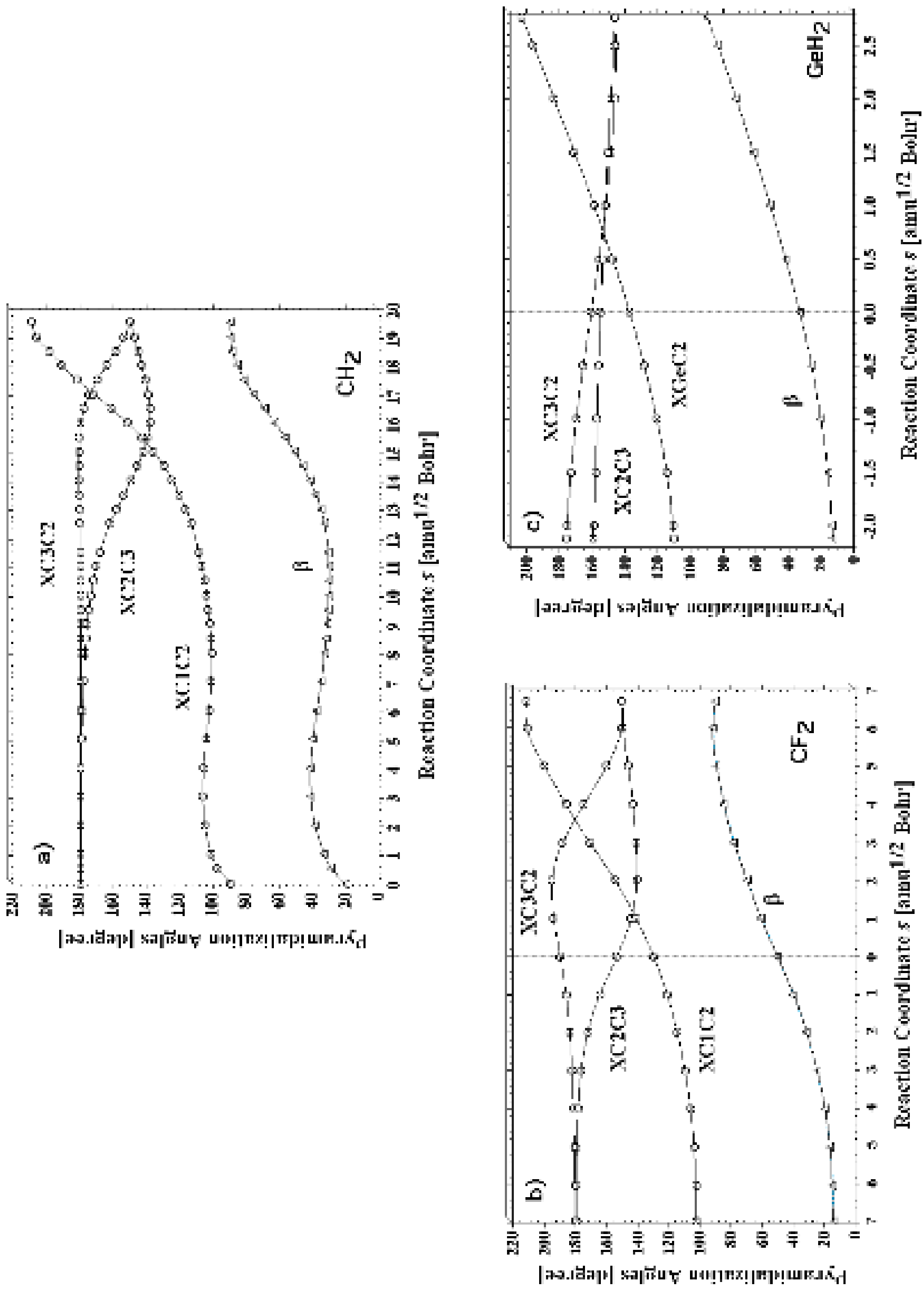

Figure 5. Calculated pyramidalization angles XC1C2, XC2C3, XC3C2, and orientation angle β (see Scheme 1b) as a function of the reaction path parameter s. **a)** CH_2: reaction (1); **b)** CF_2: reaction (2); **c)** GeH_2: reaction (3). Angles in degree. B3LYP/6-31G(d,p) calculations. The position of the TS (s = 0 amu$^{1/2}$ Bohr) is indicated by a dashed vertical line.

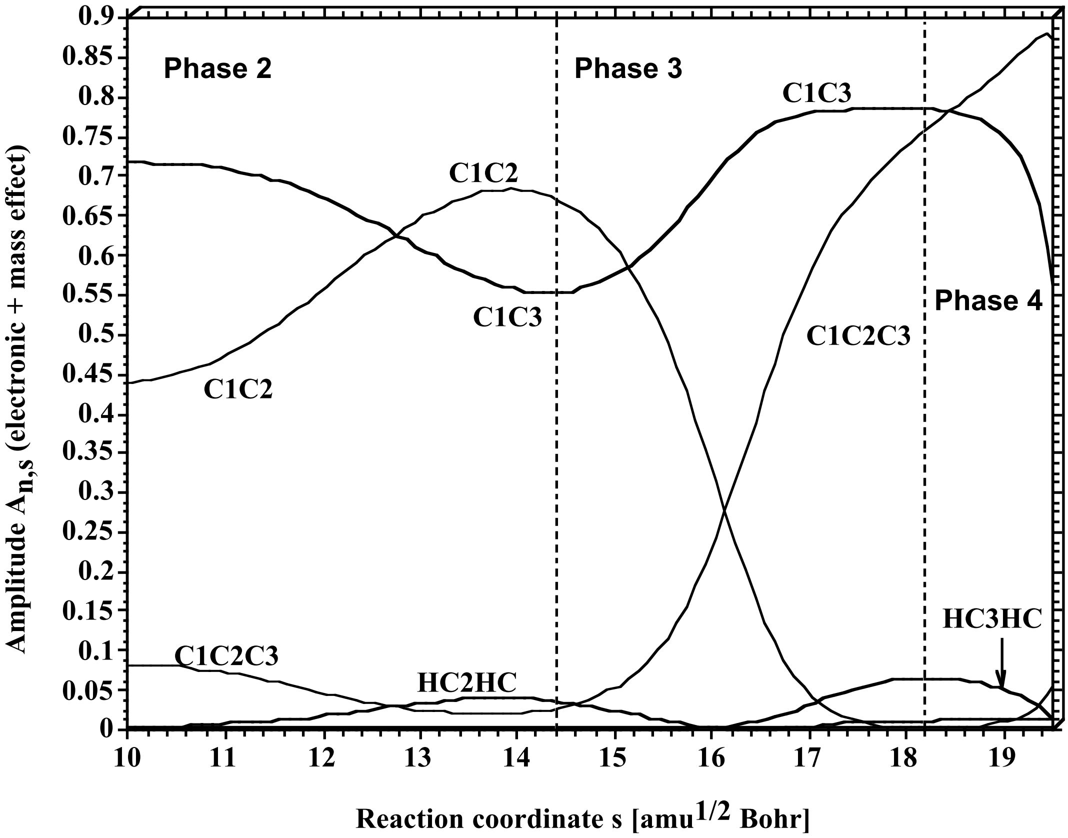

Figure 6. Characterization of the reaction path vector $\mathbf{t}(s)$ in terms of internal coordinate modes using amplitudes $A_{n,s}$ considering electronic and mass effects according to Eq. (4). For a definition of parameters, compare with Scheme 1b. The phases of the reaction mechanism are indicated by dashed vertical lines. B3LYP/6-31G(d,p) calculations.

1. Why do the van der Waals interactions between methylene and ethene not lead to a van der Waals minimum? If this would be the case, a TS should result separating reactants and product by an energy barrier.

2. Can the current analysis be used to predict the location of a TS for other chelotropic carbene additions?

3. Is it possible to enforce by appropriate substitution or environmental effects an intermediate with biradical character.

Questions 1 and 2 are relatively easy to answer on the basis of the mechanistic analysis of reaction (1): Reaction (1) is in each phase stabilizing the reaction complex. Van der Waals interactions orient the partners in such a way that the empty 2pπ(C1) orbital overlaps sufficiently with the ethene π MO and negative charge can flow from the base to the apex of the reaction complex. Non-linear carbenes possess always a permanent dipole moment and if not sterically hindered will always prefer the sideward, tail-on approach because it guarantees stabilizing interactions with ethene (alkene). A TS would develop in the electrophilic attack range if one (or more) of four reasons hinder the charge flow from alkene to carbene: a) the carbene pπ orbital is partly occupied; b) the pπ orbital has a high energy and cannot be occupied (where this can be a result of a); c) overlap between carbene pπ orbital and alkene π MO is weak and does not support charge transfer; d) the alkene is electron-poor because of electron-withdrawing substituents and therefore cannot donate electrons.

A carbene, which fulfills a), b), c) is $CF_2(^1A_1)$ (reaction (2), Scheme 1a). Because of the σ-withdrawing and π-donating nature of F, the 2pπ(C1) orbital is partly occupied, its energy is higher, and the overlap with the π(ethene) MO is because of orbital contraction at C1 reduced. It is likely that van der Waals stabilization of the reaction complex (2) lowers first the energy before hindering of charge transfer raises the energy again. This energy will be needed for rehybridization and charge reorganization so that bonding CC interactions can be established. From thereon, backdonation should start and the energy should be lowered again. In other words we expect the TS to appear when the change from electrophilic to nucleophilic phase occurs. In the case of reaction (1) this was at $s = 14.4$ amu$^{1/2}$ Bohr, which would mean that this point can be considered as a *hidden transition state (hidden TS)*, which becomes a real TS as soon as electronic or environmental effects hinder the changes of the reaction complex taking place in phase 2. We will test this hypothesis in the next section.

4. Mechanism of the Chelotropic Addition of Difluoromethylene to Ethene

The reaction $CF_2(^1A_1)$ + $H_2C{=}CH_2$ (reaction 2, Scheme 1a) is a two step reaction. [22,26-30] The reaction partners form first a van der Waals complex (Figure 3b) which, according to G3 calculations, is 1.4 kcal/mol lower in energy than the energy of the reaction partners (Table 1). The chelotropic addition step has to surmount a barrier of 9.5 kcal/mol (CCSD(T)/B) and is exothermic by 47.7 kcal/mol (G3, Table 1). After including BSSE corrections and calculating vibrational and temperature corrections, the van der Waals complex is just 0.9 kcal/mol stable, which means that it has no chemical relevance. B3LYP with either the small basis A or the large basis B and MP2/B provide reasonable descriptions of the energetics of reaction (2). Our results agree with the available experimentally based estimate of the reaction enthalpy (-47 kcal/mol, [26] Table 1) and the energy data obtained in previous quantum chemical investigations. [22,26-30]

We used the existence of a van der Waals complex to skip the investigation of phase 1 of the total reaction path. The latter was explored between s = -6.95 (position of the van der Waals complex in the entrance channel of the reaction) and $s = 6.7$ amu$^{1/2}$ Bohr (position of difluorocyclopropane in the exit channel) with $s = 0$ amu$^{1/2}$ Bohr being the location of the TS. We found a somewhat more stable (B3LYP/B: -0.05 kcal/mol) van der Waals complex of C_s-symmetry but a mirror plane passing through C1 and the C2C3 bond center, which is obtained from the van der Waals complex of Figure 3b by 90°-rotation via a small TS.

Table 1. Energies (E, ΔE) and enthalpies ($\Delta H(298)$) for reactions (1), (2), and (3). [a]

Method	Reaction (1)		Reaction (2)				Reaction (3)			
Stat. Point	Reactants	Product	Reavtants	Inter-mediate	TS	Product	Reactants	Intermediate	TS	Product
B3LYP/A, E	-117.7256	-112.1	-316.28356	-1.4	9.4	-52.0	-2154.72189	-24.4	1.5	-28.8
H		-105.5		-0.8	9.6	-48.7		-22.0	0.8	-26.4
B3LYP/B, E	-117.77254	-105.6	-316.41266	-0.4	11.3	-47.9	-2156.78329	-16.7	2.8	-18.9
H		-99.3		0.8	11.6	-44.2		-13.6	2.0	-16.0
MP2/B, E	-117.49685	-119.5	-315.899617	-1.9	11.4	-59.4	-2155.49006	-13.9[b]	2.6[b]	-36.9; -16.4[b]
H		-113.5		-0.7	11.0	-57.7		-10.5[b]	2.6[b]	-34.5; -12.4[b]
CCSD(T)/B, E	-117.50119	-107.1	-315.85763	-1.7	9.3	-50.8	-2155.01001	-18.7	0.4	-25.3
H		-100.8		-0.5	9.6	-49.1		-15.6	-0.4	-22.4
G3, E	-117.57755	-108.9	-316.20652	-1.4	NA	-52.2		NA	NA	NA
H		-100.8		-0.9	NA	-47.7		NA	NA	NA
Exp.[c]		-109.7								
		-101.6				47				-22

[a] Absolute Energies in Hartree, energy differences ΔE and enthalpy differences ΔH in kcal/mol. For CCSD(T) vibrational and thermal corrections were taken from either DFT or MP2 results. Relative energies (enthalpies) of intermediate and product are given with respect to the reactants, whereas TS energies (enthalpies) are given with respect to the intermediate. Basis A: 6-31G(d,p): basis B: 6-311++G(3df,3pd). NA: not available. [b] MP2 did not lead to an intermediate or a TS. The MP4 energies (enthalpies) are from Ref. [30]
[c] Experimental results from Ref.s [48,.49] in the case of (1) where the ΔE value was calculated with the help of the calculated vibrational and thermal corrections. The values for reactions (2) and (3) are thermochemical estimates from Ref.s [26] and [30], respectively.

A similar result was obtained by Sakai. [30] Since the PES is very flat in this direction, we did exclude the second van der Waals complex into our mechanistic analysis.

The dipole moment of $CF_2(^1A_1)$ (B3LYP/A: 0.59 Debye) is 1.2 Debye smaller than that of $CH_2(^1A_1)$, however oriented in the same direction. In view of the electronegativity of the F atoms this may be surprising if one does not consider the orientation of the group dipole moments in the molecule. The dipole moment of the C1 electron lone pair has its positive end at C1 and its negative end at the centroid of the lone pair charge. The sum of the CF bond dipole moments is oriented into the opposite direction (C1: positive end; midpoint between the F atoms: negative end; opposite polarization of σ- and π-electrons of the CF bonds reduces its value) thus leading to a partial cancellation of the group dipole moments and a smaller molecular value dominated by the lone pair orientation. Because of the smaller dipole-dipole interactions (compared with those described for reaction (1)), only a weak van der Waals complex is obtained, which however determines the starting configuration of reaction complex (2) in a similar way as found for complex (1) (Figure 3b).

The scalar path curvature for reaction (2) and its decomposition in terms of adiabatic curvature couplings is shown in Figure 7. The similarity of the curvature diagrams for reactions (1) (Figure 2) and (2) (Figure 7) is obvious despite the fact that reaction (2) is following a 2-step mechanism with intermediate and TS. Again, there are three curvature enhancements (peaks) K1, K2, K3, which are centered in phases 2, 3, and

4 of the mechanism where again the phase borders are determined by the minimums of the scalar curvature. Peak K1 at - 2 amu$^{1/2}$ Bohr indicates a short electrophilic range of 2.5 amu$^{1/2}$ Bohr and can be compared with the curvature peak K1 at s = 12.6 in the curvature diagram of reaction (1) (Figure 2). At these path points, the two carbenes are in similar positions relative to ethene as is reflected by the pyramidalization angle XC1C2 (CH_2: 114; CF_2; 114.7°, Figures 3a, 3b, 5a, and 5b), distances C1C2 (2.15; 2.28) and C1C3 (2.74; 2.78 Å, see Figures 3a and 3b) and the fact that charge transfer from ethene to carbene is a both points close to being maximal (Figures 4a and 4b).

Contrary to reaction complex (1), the charge transfer from ethene to the attacking carbene is by 40% reduced in the case of the complex positioned at K1. This confirms that the electrophilic attack of CF_2 is less pronounced than for CH_2 because of the π-donating character of the F atoms. At s = -0.6 amu$^{1/2}$ Bohr phase 2 terminates and leads over to the nucleophilic phase 3. Hence, the transition between the two phases is close to the TS and confirms that the latter is related to the curvature minimum between enhancements K2 and K3 where the minimum indicates increasing back-donation of charge from carbene to ethene (see Figures 4a and 4b).

The nucleophilic phase 3 is much more pronounced in reaction (2) compared to (1) as is reflected by a) a 30 kcal/mol decrease in energy, b) a larger curvature enhancement K2, and c) a significantly stronger charge transfer (110 melectron compared to just 10 melectron in the case of (1), see Figures 4a and 4b). At the end of phase 3, again a trimethylene biradical structure is formed characterized by a C1C3 distance of 1.872 Å (C1C2: 1.472 Å, Figure 3b). Bernardi and co-workers [28] found a weakly stable biradical intermediate at the CAS-MCSCF level of theory, which however vanished when more complete quantum chemical methods (MR-MP2) were applied. In the calculations carried out in this work, no indication of an intermediate was found on the PES, however the URVA analysis clearly identifies a hidden intermediate of biradical character at the end of the nucleophilic phase between curvature peaks K2 and K3 (Figures 3b and 7).

The reaction is terminated in phase 4, which again corresponds to ring closure of the trimethylene structure. The curvature decomposition (Figure 7) reveals that C1C3 (or alternatively C1C2C3) dominate K3 with sizable contributions however also from C1C2 and C2C3 (both being negative, resisting structure changes of the reaction complex) or CF, FCF, and the pyramidalization angles. Difluorocyclopropane (formed at s = 6.7 amu$^{1/2}$ Bohr) is characterized by a substantial donation of negative charge (40 melectron, Figures 3b and 4b) from the b_2-symmetrical pπ(F) orbitals into the $\pi^\star$ MO of the ethene unit (together they form the antibonding Walsh orbital of the three-membered ring) thus lengthening bond C2C3 to 1.548 Å and increasing the ring strain. Accordingly the exothermicity of reaction (2) is reduced by more than 50 % (Table 1).

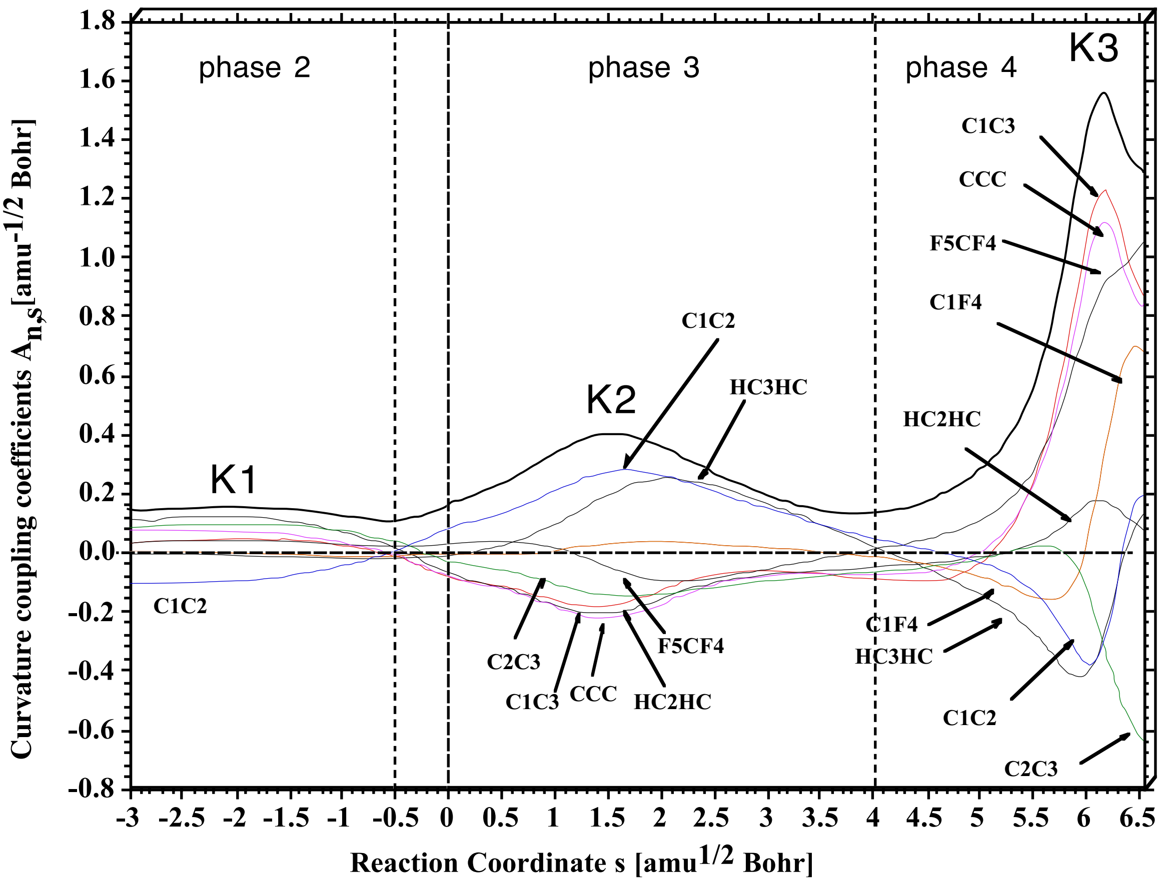

Figure 7. Decomposition of the scalar reaction path curvature κ(s) (thick solid line) in terms of adiabatic mode-curvature coupling amplitudes $A_{n,s}$(s) (thin lines). A redundant coordinate set was used for the analysis (see Scheme 1b). Curvature peaks and reaction phases are indicated. The position of the TS corresponds to $s = 0$ amu$^{1/2}$ Bohr and is indicated by a dashed vertical line. B3LYP/6-31G(d,p) calculations.

Reactions (1) and (2) follow the same 4-phase mechanism where however due to the electronic nature of CF_2 the electrophilic step is aggravated thus leading to a barrier and a TS. In a detailed and illuminating investigation of carbenes CZ_2 (Z = F, Cl, OH) Houk and co-workers [26,27] came to the same conclusions when considering the TSs of the chelotropic carbene addition reactions. Our work reveals that the investigation of just the stationary points along the reaction path is not sufficient for a reliable determination of the reaction mechanism. A TS may or may not be located in the path region where the chemical processes take place in a reaction. For example, it is outside the TS region in the preparation region in the case of the Diels-Alder reaction. In reaction (1), a TS does not exist and the reaction mechanism is characterized by the position of the curvature peaks whereas in reaction (2) the TS is located in a region where the electronic structure of the reaction complex reorganizes from a electrophilic to a nucleophilic interaction. This path region happens to be decisive for the height of the reaction barrier and therefore an analysis of the TS leads to similar conclusions than the URVA analysis. This coincidence is the reason why the mechanistic work by Houk and co-workers [26,27] led to an excellent description of important features of the mechanism of halocarbene addition reactions such as (2). We will however show in Section (5) that in a case where such a coincidence is no longer given, a TS analysis can no longer provide a description of the reaction mechanism.

In none of the previous investigations, the mechanism of reaction (1) was analyzed in detail and used for predicting the mechanism of other carbene addition reactions with a totally different energy profile as done in this work for reaction (2). We will extend this test to the more difficult problem of reaction (3) and see whether despite the large differences between reactions (1) and (3) the mechanism of the latter can be predicted on the basis of what is known for (1).

5. Mechanism of the Chelotropic Addition of Germylene to Ethene

Germylene has similar to difluorocarbene but contrary to methylene a singlet rather than a triplet ground state. Its singlet-triplet splitting has been estimated to be 23 - 24 kcal/mol on the basis of high level ab initio calculations. [52] Apeloig and co-workers have pointed out that for silylene and germylene the HOMO-LUMO gap almost doubles compared to that of methylene. This is a consequence of the electropositive character of Si or Ge, which causes a much stronger second order Jahn-Teller effect involving the a_1-symmetrical σ-type HOMO and LUMO so that the energy gap between σ-type HOMO and π-type LUMO also becomes large. Other factors such as the larger YZ bond polarity of $GeH_2(^1A_1)$ compared to that $CH_2(^1A_1)$, and the larger s-character of the a_1-symmetrical HOMO increase this difference. Any raise in the energy of the pπ-LUMO makes the electrophilic step (phase 2) in the chelotropic addition reaction more difficult, but will not exclude this as long van der Waals interactions position germylene in a similar way as the carbenes in reactions (1) and (2).

$GeH_2(^1A_1)$ possesses an even smaller dipole moment (0.26 Debye) than that of CF_2, which in addition is oriented opposite to that of methylene. Magnitude and direction are a result of opposing lone pair and GeH_2 group moments. Since the GeH bonds are polarized toward the more electronegative H atoms (Pauling electronegativities of H and Ge: 2.54 and 2.01 [51]) and the lone pair dipole moment is smaller due to increased s-character, the orientation of the dipole moment is from Ge (positive end) to the H atoms (negative end). In view of the small dipole moment, there is no chance of forming a van der Waals complex in reaction (3), however even a small dipole moment is sufficient to orient the reactants in a way that supports an electrophilic attack. The position of GeH_2 is shifted more to the center of the C2C3 double bond so that the (partly positively charged) Ge atom is close to C2 and C3 and the (partly negatively charged) H atoms are closer to the H atoms of C3 (see Figure 3c).

The data of Table (1) reveal that reaction (3) proceeds similar to reaction (2) via a 2-step mechanism. In the first step a biradicaloid (Figure 3c) is formed which closes in the second step via a small barrier to the three-membered ring. The biradicaloid corresponds to the TS structure detected in reactions (1) and (2) between phases 2 and 3. We prefer however the term biradicaloid because distance GeC2 (2.147 Å, Figure 3c) is already close to that of a normal GeC bond length and the notation of a TS does not fit to the description of a local minimum. However, we stress that the biradicaloid is related to the TS structures between phases 2 and 3 detected for (1) and (2).

The biradicaloid is calculated to be 18.7 (CCSD(T)) more stable than the reactants. Depending on the level of theory applied a barrier of 0.4 (CCSD(T)) to 2.8 kcal/mol (B3LYP/B, Table 1) results, which after vibrational and temperature corrections either vanishes or is reduced to a small value in the 1 - 2 kcal/mol range. Similar as in the case of reaction (2), intermediate and TS have no chemical relevance, however help to define a unique path, which is representative of all other energy-favorable paths. Reaction (3) is exothermic by 25.3 kcal/mol (CCSD(T)), which is comparable to the B3LYP results (Table 1), however differs by 10 kcal/mol from either MP2 or MP4 results (see also Ref, [30]). MP2 does not lead to an intermediate or a TS because it exaggerates the exothermicity of the reaction. In summary, reaction (3) is the least exothermic of the three chelotropic addition reactions investigated, its exothermicity being just 25 % of that of reaction (1).

Reaction path (3) was followed from the position of the biradicaloid at s = -2.12 amu$^{1/2}$ Bohr down to the position of the three-membered ring at s = 2.76 amu$^{1/2}$ Bohr, which already indicates that the reaction path is short stretching just over 4.9 amu$^{1/2}$ Bohr. Considering the fact that only 10 to 25 % (depending on the method used) of the reaction energy of (3) is recovered from the calculated reaction path (see Table 1), it is likely that the path length from the reactants to the biradicaloid is substantial and comprises again a van der Waals phase (although not a stationary point corresponding to a van der Waals complex as found for reaction (2)) and an electrophilic attack phase leading to the biradicaloid at s = -2.12 amu$^{1/2}$ Bohr.

In Figure 8, the scalar path curvature and its decomposition in terms of adiabatic curvature couplings is shown for reaction (3). The curvature diagram differs from those of reactions (1) (Figure 2) and (2) (Figure 7) in so far as just two curvature peaks (K2 and K3) rather than three are found in line with the fact that the reaction path starts with phase 3 rather than 2 or even 1. Contrary to reaction (2), the TS is shifted from a position between K1 and K2 to a new one between K2 and K3. Investigation of charge transfer (Figure 3c: strong transfer of negative charge from GeH_2 to ethene in the sense of a nucleophilic attack) and changes in the pyramidalization angles (Figure 5c) confirms that K2 is located in phase 3 and associated with the nucleophilic attack of germylene on ethene. The TS is located after K2 close to the minimum of scalar curvature at s = 0.5 amu$^{1/2}$ Bohr. It represents now the transition from the nucleophilic attack to the ring closure range (compare with Figure 3c).

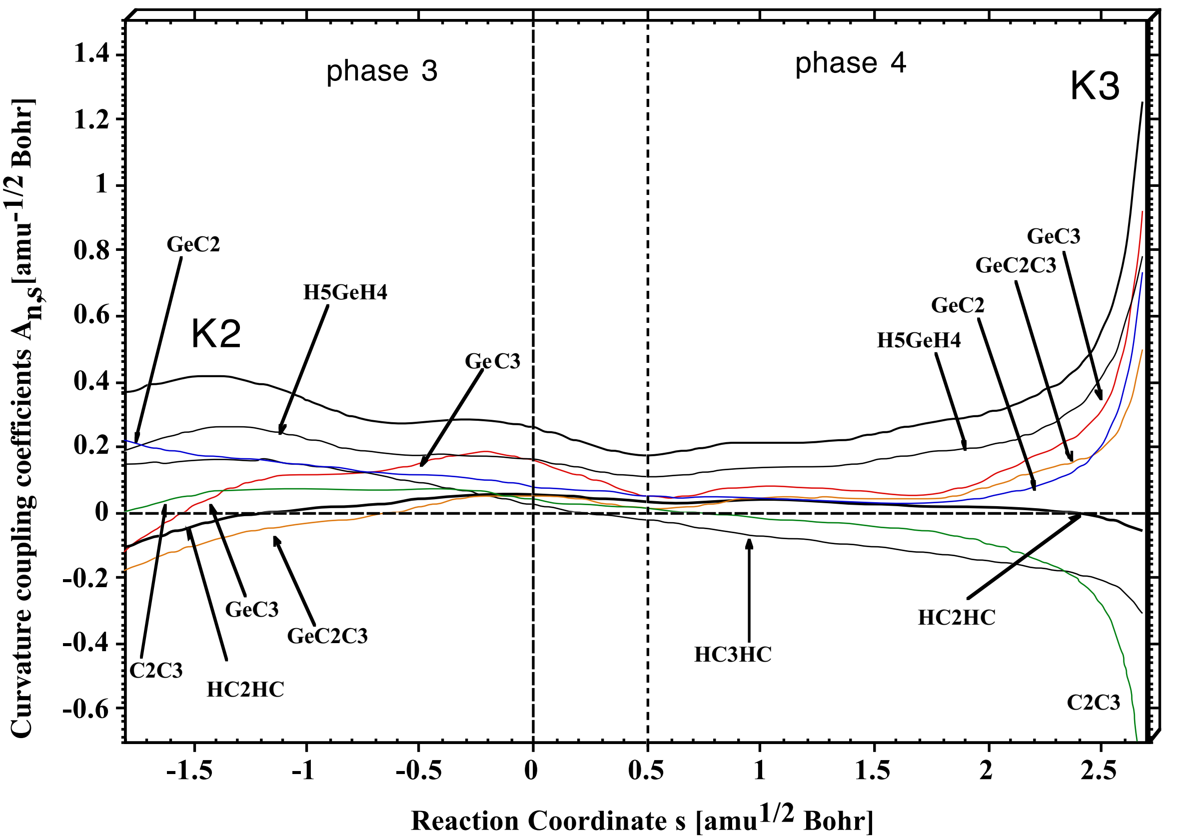

Figure 8. Decomposition of the scalar reaction path curvature $\kappa(s)$ (thick solid line) in terms of adiabatic mode-curvature coupling amplitudes $A_{n,s}(s)$ (thin lines). A redundant coordinate set was used for the analysis (see Scheme 1b). Curvature peaks and reaction phases are indicated. The position of the TS corresponds to $s = 0$ amu$^{1/2}$ Bohr and is indicated by a dashed vertical line. B3LYP/6-31G(d,p) calculations.

The ring closure phase stretches over 2.2 amu$^{1/2}$ Bohr and leads to a lowering by just 2 kcal/mol (Figure 3c) indicating that the biradical structure at $s = 0.5$ is already close to GeC3 bond formation. The largest contributions to curvature peak K3 stem from the adiabatic stretching or bending modes GeC3, HGeH (positive and thereby supporting geometry changes of the reaction complex), and C2C3 (negative and thereby resisting geometry changes). Germirane (germacyclopropane) has a higher strain energy (37 kcal/mol) than cyclopropane (27 kcal/mol), [30,54,55] however the difference (10 kcal/mol) is not that large to explain the much lower exothermicity of the reaction. There are two other reasons, which are responsible for the reduced exothermicity of the reaction. a) In its singlet ground state, GeH_2 (compared to the GeH_2 group in H_3Ge-GeH_2-GeH_3 via the reaction GeH_2 + H_3Ge-GeH_3 $\rightarrow$ H_3Ge-GeH_2-GeH_3) is more stable than CH_2 in its singlet excited state (compared to the CH_2 group in propane). b) The GeC bonds formed in the reaction are relatively unstable [30,51] and compensate less the loss of the double bond of ethene. In addition bond C2C3 is significantly weakened in germirane due to the transfer of negative charge from the germanium b_2 symmetrical orbital into the $\pi^\star$ orbital of the ethene unit, which together form of course the antibonding Walsh orbital. [56] The consequences of the charge transfer are reflected by a lengthening of C2C3 bond to 1.533 Å (Figure 3c).

It remains to be asked why a TS is established at all because, on the basis of the arguments considered so far, reaction (3) should proceed barrierless although with a strongly reduced exothermicity. It is easy to see that despite much lower electrostatic interactions in phase 1 and a high lying 4pπ(Ge) orbital, electrohilic charge transfer in phase 2 will proceed similar as in reaction (1), i.e. without the formation of a van der Waals complex. The energy of the germylene LUMO plays however a role when entering the nucleophilic attack range. In this range rehybridization at the Ge atom and repopulation of the orbitals is essential to strengthen bond GeC2 and start the formation of bond GeC3. This step is energetically hampered by the fact that a higher lying LUMO makes rehybridization and charge redistribution more difficult than in the case of reactions (1) and (2) thus leading to a TS at the end of phase 3. This was foreseeable when considering the properties of germanium and led to the choice of reaction (3) as an example with a TS shifted from the end of the electrophilic phase (reaction 2) to the end of the nucleophilic range. It is sufficient to know the mechanism of the parent reaction (1) to predict changes in the mechanism for other carbenes, silylenes, germylenes, etc.

6. Chemical Relevance of Results and Conclusions

The URVA analysis of the chelotropic addition reaction between ethene and methylene (reaction 1) reveals that a barrierless reaction can possess a complicated, multi-phase reaction mechanism. In the case of reaction (1), the reaction complex passes through four different phases:

a) In the van der Waals phase, the first electrostatic interactions between the reaction partners are established, which decide on the orientation of the incoming methylene and the configuration of the reaction complex. The detailed analysis does not confirm that the non-linear, sideward approach of methylene is a result of charge-transfer from ethene to methylene involving π(ethene) and 2pπ(CH_2) MO. The configuration of the reaction complex is a result of dipole-induced dipole interactions taking place before any charge can be transferred. The charge transferred is a consequence rather than the cause of the orientation of the reaction partners. Although the the stabilizing interactions lead to an energy gain of just a couple of kcal/mol (less than 2% of the total reaction energy), the stereochemistry and by this the fate of the reaction complex is determined in the van der Waals region. This was not considered in previous investigations of reaction (1).

b) A number of path and reaction complex properties indicate the end of the van der Waals region and the transition to the electrophilic attack region, in which methylene withdraws negative charge from ethene via overlap between the π(ethene) and 2pπ(CH_2) MOs. The electrophilic attack range stretches over 50% of the total reaction path, which is in line with slow electronic, geometrical, and dynamic changes of the reaction complex. In previous work [4,5] we have found that for symmetry-forbidden reactions isolated parts of the reaction complex change drastically whereas in symmetry-allowed reactions a collective change of many geometric parameters slowly prepares the reaction complex for the actual chemical processes (bond forming or breaking) of the reaction. This does not require large energies and is the major reason why symmetry-allowed reactions possess relatively low barriers or, as in the case of (1) do not have a barrier at all.

c) At the end of phase 2, a maximal charge transfer between the reaction partners is reached and the direction of charge transfer is inverted. This indicates the transition from the electrophilic to the nucleophilic phase of reaction (1). A number of significant changes in the electronic structure and the geometry of the reaction complex cause by rehybridization and redistribution of negative charge take place within the a relatively short range of the path that establish a distorted trimethylene biradical structure.

d) In the last phase of the reaction mechanism the trimethylene structure is closed to the three-membered ring by forming bond C1C3 and adjusting all bond parameters to the D_{3h} symmetry of the ring.

We observe two distinct intermediate structures of the reaction complex (1), which can be identified and characterized although they are not associated with any stationary point. The first resembles a TS for C1C2 bond formation and is located at the end of the electrophilic reaction phase. We call this structure a hidden TS because it changes to a real TS when replacing the H atoms by F atoms (reaction 2).

The second intermediate structure is found at the end of the nucleophilic phase and corresponds to a hidden biradical intermediate with a distorted trimethylene structure. Although we have not discussed in this work the conversion of this hidden intermediate into a real intermediate, it is easy to predict that steric interactions between bulky carbene and/or alkene substituents will hinder C1C3 bond formation and ring closure of the trimethylene intermediate. Bernardi and co-workers [28] have discussed this aspect in their work on the difluorocarbene-ethene system and we can follow their line of argument although the expected biradical intermediate found for reaction (2) in their work cannot be confirmed by the calculations carried out in this work.

Extending these ideas, it is reasonable to expect also a hidden intermediate located at the transition from van der Waals region to electrophilic attack region. Clearly such a hidden intermediate converts to a van der Waals complex when electronic or environmental effects stabilize its structure. For reaction (2), this situation occurs, however not in a way that increased van der Waals interactions lead to the occurrence of a van der Waals complex. On the contrary, van der Waals interactions are reduced for (2), but this causes changes in the reaction complex, which hamper the following electrophilic attack so that a higher energy is needed. This leads to the establishment of a TS, which implies the formation of a local minimum at the transition from phase 1 to phase 2 of (2).

It remains to answer the question whether in general any transition from one reaction phase to another (primarily indicated by the reaction path curvature diagram) is the location of a hidden TS or a hidden intermediate. Future investigations have to clarify this point where one has to consider that real TSs are seldom located at positions of mechanistic transitions. We have coined the term *transition state region* [1,2] to distinguish between the reaction phase, in which the chemical processes occur and the energetic TS, which is seldom located at the center of the TS region. It may be even outside the TS region as found for the Diels-Alder reaction. [5]

Knowledge of hidden intermediates and hidden TS makes it possible to anticipate changes in the number of stationary points encountered along the reaction path and the energetics of a reaction. Once the mechanism of reaction (1) is understood, the appearance of intermediate and TS for reactions (2) and (3) can be anticipated. Reaction (2) was chosen to establish a van der Waals complex at the end of phase 1, which implies a TS at the end of phase 2. Reaction (3) is an example for a 4-phase mechanism with biradicaloid intermediate and a TS at the end of the nucleophilic step.

In which future work, we will investigate whether the mechanism of reaction (1) is still valid when seemingly different carbenes such as vinylidene react with alkenes or even alkines. As we have already found in ongoing work for the reaction between vinylidene and acetylene this seems to be largely the case. Apart from this we have to clarify whether all symmetry-allowed pericyclic reactions of the chelotropic type possess similar mechanisms. There is evidence that there are larger similarities between certain reactions which according to established chemical knowledge are considered to be basically different.

The results of this work suggest that reaction mechanism must be understood in a more fundamental way than done so far in order to be able to effectively control chemical reactions.

Acknowledgment

EK and DC thank the University of the Pacific for supporting this work.

References

[1] E. Kraka, in *Encyclopedia of Computational Chemistry*, P.v.R. Schleyer, N.L. Allinger, T. Clark, J. Gasteiger, P.A. Kollman, H.F. Schaefer III, P.R. Schreiner, Eds., Wiley, Chichester, (1998), Vol 4. p2437.

[2] Z. Konkoli, E. Kraka and D. Cremer, *J. Phys. Chem. A*, **101**, 1742 (1997).

[3] Z. Konkoli, D. Cremer, and E. Kraka *J. Comput. Chem.* **18**, 1282 (1997).

[4] D. Cremer D, A. Wu, and E. Kraka, *Phys. Chem. Chem. Phys.*, **3**, 674 (2001). 1706.

[5] E. Kraka, A. Wu, and D. Cremer *J. Phys. Chem. A.*, **107**, 9008 (2003).

[6] E. Kraka, and D. Cremer *J. Phys. Org. Chem.*, **15**, 431 (2002).

[7] W.H. Miller, N.C. Handy, J.E. Adams, *J. Phys. Chem. A*, **72**, 99 (1980).

[8] K. Fukui, *J. Phys. Chem.*, 1970, **74**, 4161.

[9] K. Fukui, *Acc. Chem. Res.*, **14**, 363 (1981).

[10] (a) Z. Konkoli and D. Cremer, *Int. J. Quant. Chem.* **67**, 1 (1998); (b) Z. Konkoli,L.A. Larsson,and D. Cremer, *Int. J. Quant. Chem.* **67**, 11 (1998); (c) Z. Konkoli,L.A. Larsson,and D. Cremer, *Int. J. Quant. Chem.* **67**,291 (1998).

[11] D. Cremer, L.A. Larsson, and E. Kraka, in *Theoretical and Computational Chemistry, Vol. 5, Theoretical Organic Chemistry*, ed. C. Párkányi, Elsevier, Amsterdam, (1998), p.259.

[12] (a) K. Morokuma and S. Kato. In *Potential Energy Characteristics for Chemical Reactions*, D.G. Truhlar, Ed., Plenum Press, New York, (1981), 243; (b) W.H.Miller. In *The Theory of Chemical Reaction Dynamics*, C.D. Clary CD, Ed., Reidel, Dordrecht, (1986), p27; (c) D G. Truhlar and B. Garrett, *Annu. Rev. Phys. Chem.*, **35**,159 (1986); (d) D.G. Truhlar, R. Steckler, and M. Gordon, *Chem. Rev.*, **87**, 217 (1987); (e) D.G. Truhlar, F. Brown, R. Steckler, and A.D. Isaacson. In *The Theory of Chemical Reaction Dynamics*, C. D. Clary, Reidel: Dordrecht, (1986), 285.

[13] E. Kraka E and T.H. Dunning Jr. In sl Advances in Molecular Electronic Structure Theory: the Calculation and Characterization of Molecular Potential Energy Surfaces, T.H. Dunning THJr., Ed., JAI Press, Greenwich, CT, 1990; 129.

[14] W. Quapp, E. Kraka, anad D. Cremer, *J. Phys. Chem. A*, in press.

[15] W. Quapp, M. Hirsch, O. Imig, and D. Heidrich, *J. Computat. Chem.*, **19**, 1087 (1998).

[16] a) M. Hirsch and W. Quapp, *J. Mol. Struct. THEOCHEM*, **683**, 1 (2004); b) W. Quapp, *J. Mol. Struct.*, **95**, 695 (2004).

[17] P.S. Skell, and A.Y. Garner, *J. Am. Chem. Soc.*, **78** 5430 (1956).

[18] W.E. von Doeringa and W.A. Henderson, *J. Am. Chem. Soc.*, **80** 5274 (1958).

[19] P.S. Skell and M.S. Cholod, *J. Am. Chem. Soc.*, **91** 7131 (1969), and references therein.

[20] R.A. Moss, in *Carbenes*, M. Jones and R.A. Moss, Eds., Wiley, New York, (1973), Vol. I.

[21] R. Hoffmann, *J. Am. Chem. Soc.*, **90**, 1475 (1968).

[22] R. Hoffmann, D.M. Hayes, and P.S. Skell, *J. Phys. Chem.*, **76** 664 (1972).

[23] B. Zurawski, and W. Kutzelnigg, sl J. Am. Chem. Soc. , **100**, 2654 (1978).

[24] F. Bernardi, and M. A. Robb, *J. Am. Chem. Soc.*, **106**, 54 (1984).

[25] M. Sironi, M. Raimondi, D.L. Cooper, and J. Gerratt, *J. Chem. Soc. Faraday Trans. 2*, **83**, 1651 (1987).

[26] N.G. Rondan, , K.N. Houk, R.A. Moss, *J. Am. Chem. Soc.*, **1980**, *102, (1770).*

*[27] K.N. Houk, N.G. Rondan, and J. Mareda, J. J. Am. Chem. Soc.,***106** *(1984).*

[28] F. Bernardi, A. Bottoni, C. Canepa, M. Olivucci, M.A. Robb, M. A., G. Tonachini, J. Org. Chem. **62**, *1018 (1997).*

[29] J.J. Blavins, D.L. Cooper, and P.B. Karadako, Int. J. Quant. Chem., **98**, *465 (2004).*

[30] S. Sakai, Int. J. Quantum. Chem., bf 70, 291 (1998).

[31] R.B. Woodward and R. Hoffmann Angew. Chem. Int. Ed. Engl, 1969, **8**, *781.*

[32] A. E. Keating, S.R. Merrigan, D.A. Singleton, K.N. Houk, J. Am. Chem. Soc., **121**, *3933 (1999).*

[33] For a review see D. Cremer, in Encyclopedia of Computational Chemistry, eds. P.v.R. Schleyer, N.L. Allinger, T. Clark, J. Gasteiger, P.A. Kollman, H.F. Schaefer III, P.R. Schreiner, Wiley, Chichester, (1998), Vol.3, p1706.

[34] (a) P. Hohenberg, and W. Kohn, Phys. Rev, **136**, *B864 (1994) ; (b) W. Kohn, and L. Sham, J. Phys. Rev.* **140**, *A1133 (1965). See also (c) R. G. Parr and W. Yang, International Series of Monographs on Chemistry 16: Density-Functional Theory of Atoms and Molecules, Oxford University Press, New York, (1989).*

[35] For a review see (a) J. Gauss, in Encyclopedia of Computational Chemistry, eds. P.v.R. Schleyer, N.L. Allinger, T. Clark, J. Gasteiger, P.A. Kollman, H.F. Schaefer III, P.R. Schreiner, Wiley, Chichester, (1998), Vol.1, p615; (b) T.D. Crawford and H.F. Schaefer III in Reviews in Computational Chemistry, Vol. 14, K.B. Lipkowitz, D.B. Boyd, Eds, Wiley-VCH, Weinheim, (2000) p33.

[36] K. Raghavachari, G.W. Trucks, J.A. Pople and M. Head-Gordon, Chem. Phys. Lett., **157**, *479 (1989).*

[37] G3: L.A. Curtiss, K. Ragshavachari, P.C. Redfern, V. Rassolov, and J.A. Pople, J. Chem. Phys., **109**, *7764, (1998). G2: L. A. Curtiss, K. Raghavachari, G.W. Trucks and J.A. Pople, J. Chem. Phys.,* **94**, *7221 (1991).*

[38] P.C. Hariharan and J.A. Pople, Theoret. Chim. Acta, **28**, *213 (1973).*

[39] R. Krishnan, R., M. Frisch, and J.A. Pople, J. Chem. Phys., **72**, *4244 (1980).*

[40] (a) A.D. Becke, J. Chem. Phys. **98**, *5648 (1993). See also (b) J.P. Stevens, F.J. Devlin, C.F. Chablowski and M.J. Frisch, J. Phys. Chem.,* **98**, *11623 (1994).*

[41] *See, e.g., J. Baker, M. Muir, J. Andzelm and A. Schreiner in Chemical Applications of Density Functional Theory, ACS Symposium Series 629, B.B. Laird, B.B., R.B Ross, and T. Ziegler, Eds., American Chemical Society: Washington, DC, (1996), p342.*

[42] *N.R. Kestner and J.E. Comariza, in Reviews in Computational Chemistry, Volume 13, K.B. Lipkowitz and D.B. Boyd, Eds., Wiley-VCH, New York, (1999), p99.*

[43] *F. Boys and F. Bernardi, Mol. Phys.,* **19**, *553 (1970).*

[44] *A.E. Reed, L.A. Curtiss, and E. Weinhold, Chem. Rev.,* **88**, *899 (1988).*

[45] *E. Kraka, J. Gräfenstein, M. Filatov, A. Wu, H. Joo, D. Izotov, J. Gauss, Y. He, Z. He, V. Polo, F. Reichel, Z. Konkoli, L. Olsson, D. Cremer COLOGNE 2007, University of the Pacific, 2007.*

[46] *Gaussian 03, Revision C.02, M. J. Frisch, G. W. Trucks, H. B. Schlegel, G. E. Scuseria, M. A. Robb, J. R. Cheeseman, J. A. Montgomery, Jr., T. Vreven, K. N. Kudin, J. C. Burant, J. M. Millam, S. S. Iyengar, J. Tomasi, V. Barone, B. Mennucci, M. Cossi, G. Scalmani, N. Rega, G. A. Petersson, H. Nakatsuji, M. Hada, M. Ehara, K. Toyota, R. Fukuda, J. Hasegawa, M. Ishida, T. Nakajima, Y. Honda, O. Kitao, H. Nakai, M. Klene, X. Li, J. E. Knox, H. P. Hratchian, J. B. Cross, V. Bakken, C. Adamo, J. Jaramillo, R. Gomperts, R. E. Stratmann, O. Yazyev, A. J. Austin, R. Cammi, C. Pomelli, J. W. Ochterski, P. Y. Ayala, K. Morokuma, G. A. Voth, P. Salvador, J. J. Dannenberg, V. G. Zakrzewski, S. Dapprich, A. D. Daniels, M. C. Strain, O. Farkas, D. K. Malick, A. D. Rabuck, K. Raghavachari, J. B. Foresman, J. V. Ortiz, Q. Cui, A. G. Baboul, S. Clifford, J. Cioslowski, B. B. Stefanov, G. Liu, A. Liashenko, P. Piskorz, I. Komaromi, R. L. Martin, D. J. Fox, T. Keith, M. A. Al-Laham, C. Y. Peng, A. Nanayakkara, M. Challacombe, P. M. W. Gill, B. Johnson, W. Chen, M. W. Wong, C. Gonzalez, and J. A. Pople, Gaussian, Inc., Wallingford CT, (2004).*

[47] *a) J. F. Stanton, J. Gauss, J. D. Watts, W. J. Lauderdale and R. J. Bartlett, ACES II, Quantum Theory Project, University of Florida, 1992; b) J.F. Stanton,J. Gauss, J., J.D. Watts, J.D., W.J. Lauderdale and R.J. Bartlett, Int. J. Quant. Chem. Symp., 1992,* **26**, *879.*

[48] *NIST Standard Reference Database 25, Version 2.02, National Institute of Standards and Technology, Gaithersburg. MD 20899 USA, (1994); (b) J.D. Cox and G. Pilcher, G. Thermochemistry of Organic and Organometallic Compounds, Academic Press, London, (1970).*

[49] *(a) G.A. Peterson and M.A. Al-Laham, J. Am. Chem. Soc,* **111**, *1256 (1989); (b) J.W. Simon and R. Curry, Chem. Phys. Lett.,* **38**, *171 (1976).*

[50] *(a) R.J. Berry, C.J. Ehlers, D.R. Burgess, Jr. M.R. Zachariah, M.R. Nyden and M. Schwartz, J. Mol. Struct. THEOCHEM,* **422**, *89 (1998); (b) T.Yamada, T.H. Lay and J.W. Bozzelli, J. Phys. Chem. A,* **102**, *7286 (1998).*

[51] CRC Handbook of Chemistry and Physics on CD-ROM, 2000 Version. ed. D.R. Lide, CRC Press LLC.

[52] (a) R. S. Grev, H. F., III Schaefer, K. M. Baines, J. Am. Chem. Soc, **112**, *9458 (1990). (b) K. J. Balasubramanian, Chem. Phys.,* **89**, *5731 (1988). (c) L. G. M. Petterson, P. E. M. Siegbahn, J. Chem. Phys.,* **105**, *355 (1986). (d) G. Olbrich, Chem. Phys. Lett.,* **73**, *110 (1980). (e) A. Selmani, D. R. Salahub, J. Chem. Phys.,* **89**, *1592 (1988). (h) K. G. Dyall, J. Chem. Phys.,* **96**, *1210 (1992).*

[53] Y. Apeloig, R. Pauncz, M. Karni, R. West, W. Steiner, D. Chapman, Organometal., **22**, *3250 (2003).*

[54] M. Su, S.-Y. Chu, J. Am. Chem. Soc., **121**, *11478 (1999).*

[55] W. Ando, H. Ohgaki, Y. Kabe, Angew. Chem. Int. Edt., **33**, *659 (2003).*

[56] D. Cremer, E. Kraka, K. J. Szabo in The Chemistry of Functional Groups, The Chemistry of the Cyclopropyl Group, Vol. 2, ed. by Z. Rappoport, Wiley, New York, 1995, p. 43.